Advances in Natural Sciences:
Nanoscience and Nanotechnology

PAPER

Biosynthesis of α-MoO_3 nanoparticles and its adsorption performance of cadmium from aqueous solutions

To cite this article: Ibrahem M A Hasan *et al* 2021 *Adv. Nat. Sci: Nanosci. Nanotechnol.* **12** 035007

IOP Publishing | Vietnam Academy of Science and Technology Advances in Natural Sciences: Nanoscience and Nanotechnology

Adv. Nat. Sci.: Nanosci. Nanotechnol. **12** (2021) 035007 (8pp) https://doi.org/10.1088/2043-6262/ac2050

Biosynthesis of α-MoO_3 nanoparticles and its adsorption performance of cadmium from aqueous solutions

Ibrahem M A Hasan, Ahmed R Tawfik and Fawzy H Assaf

Chemistry Department, Faculty of Science, South Valley University, Qena 83523, Egypt

E-mail: hasan111167@gmail.com

Received 30 March 2021
Accepted for publication 26 June 2021
Published 2 September 2021

Abstract

Molybdenum (VI) oxide nanoparticles (α-MoO_3 NPs) were green synthesised using buckthorn leaf extract as the reducing and capping agents. The α-MoO_3 NPs were characterised by thermogravimetric analysis, fourier transforms infrared spectroscopy, X-ray diffraction, field emission scanning, and transmission electron microscopy, energy-dispersive x-ray spectroscopy, and Brunauer–Emmett–Teller surface area analysis. The analyses showed the formation of spherical-shaped α-MoO_3 NPs with ~50 nm mean crystallite size, 3.825 $m^2\ g^{-1}$ surface area, and 0.005 $cm^3\ g^{-1}$ total pore volume. The synthesised α-MoO_3 was then applied for adsorption of Cd (II) from aqueous solutions. Optimisation of various adsorption parameters resulted in complete Cd (II) removal under the conditions: 0.1 g α-MoO_3 dose, 60 min contact time, 50 mg l^{-1} initial Cd (II) concentration, pH 7 and 298 K. The experimental results were further assessed using different kinetic, isotherm and thermodynamic models. The data were best described by pseudo-second-order ($R^2 = 0.992$) and Langmuir ($R^2 = 0.98$) models with a maximum adsorption capacity of 57.5 mg g^{-1} at optimum conditions. Thermodynamic results indicated that the adsorption process is feasible, spontaneous, and endothermic in nature. Moreover, upon regeneration and interference results, α-MoO_3 is stable and selective for Cd (II) adsorption in presence of other cations. Upon these results, the biosynthesised α-MoO_3 NPs can be used as a selective adsorbent for the efficient removal of Cd (II) from aqueous media.

Supplementary material for this article is available online

Keywords: Cadmium removal, adsorption, molybdenum oxide nanoparticles, buckthorn, green synthesis

Classification numbers: 2.00, 2.03, 4.00, 4.02, 5.00, 5.18

1. Introduction

As a result of the rapid advance in industry and the remarkable agricultural exercise, water bodies have been polluted with heavy metals which have adverse effects on human health and the ecosystem [1]. So, it is indispensable to intensely remove noxious metals from water resources [2–5]. Cadmium is one of the most hazardous heavy metals to human health. It is non-biodegradable, carcinogenic, and has harmful effects on kidneys and bones [5, 6]. Cadmium reaches water sources from metal mining, alloy preparation, electrolysing, and electroplating. Word Health Organization set the Cd (II) maximum allowable concentration of 0.003 mg l^{-1} in drinking water (WHO, 2011). Therefore, several Cd (II) removal strategies have been utilised such as chemical precipitation, coagulation, ion exchange, ultrafiltration, solid phase extraction, and adsorption [7–9]. Among these methods, adsorption by nanomaterials is a relevant research area, because of its cost-effectiveness, high removal efficiency, adsorbent stability, and ease of operation [2, 10–12]. An important class of nano-adsorbents is metal oxide nanoparticles (MONPs) that have been applied for the removal of Cd (II) and other heavy metals from aqueous solutions [13–16].

One of these important MONPs is molybdenum (VI) oxide nanoparticles (MoO_3 NPs) which exist in three main forms including the orthorhombic (α-MoO_3), the monoclinic (β-MoO_3), and the hexagonal phases (h-MoO_3) [17]. Among them, the stable and environmentally safe α-MoO_3 has been widely applied in various fields such as catalysis, sensors, lithium-ion batteries, organic solar cells, and display materials [17–19]. α-MoO_3 has been prepared by several physicochemical methods such as hydrothermal, electrochemical, sonochemical, thermal evaporation, chemical vapour deposition, and laser ablation methods [20–24]. However, these methods have many limitations such as high cost, harsh conditions, additional use of capping agents and stabilisers, and generation of toxic byproducts. Thus, plant-mediated biogenic synthesis of α-MoO_3 is receiving growing interest [25–28]. Buckthorn: *Christ's thorn jujube* (*CTJ*) is rich in polyphenols and has an antioxidant activity of 0.6 – 1.5 mg g^{-1} dry mass [29, 30]. In spite of all above mentioned synthesis and applications of α-MoO_3, it has not been previously prepared using CTJ or applied for removal of Cd (II) to our best knowledge. Thus, this work aimed to green synthesise α-MoO_3 NPs using buckthorn leaves and to apply it for removal of Cd (II) from aqueous solutions. The effects of α-MoO_3 NPs dose, adsorption time, Cd (II) concentration, pH, and temperature were investigated. Besides, the adsorption kinetics, isotherms, and thermodynamics were examined. The stability, selectivity, and adsorption mechanism of α-MoO_3 were also discussed.

2. Materials and methods

2.1. Materials

Sodium molybdate dihydrate ($Na_2MoO_4.2H_2O$) and cadmium (II) chloride dihydrate ($CdCl_2.2H_2O$) were purchased from Merck and used directly without pretreatment. *CTJ* leaves aqueous extract was used to synthesise α-MoO_3 NPs. All other chemicals are of analytical grade and used as received without further purification. Bi-distilled water was employed for aqueous solution preparation at ambient temperature.

2.2. Synthesis of MoO_3 NPs

The extract of buckthorn dried leaves was prepared by boiling 25 g in 100 ml bi-distilled water for 2 hrs, filtered, and employed for the reduction of sodium molybdate. The α-MoO_3 NPs were prepared by treating the salt with plant extract in a volume ratio (1:2) at ambient temperature (25 °C) under continuous vigorous stirring for an hour. The change in colour from watery to ruby red elucidates the formation of NPs. The α-MoO_3 NPs were isolated through centrifugation at 6000 rpm for 15 min followed by washing with bi-distilled water several times and drying at 80 °C overnight. The dried product was calcined at 700 °C for 3 hrs in an electric muffle furnace followed by crushing using pestle and mortar and stored in a brown sealed container.

2.3. Instruments

The thermal stability was investigated by TGA analyser (TGA 8000, PerkinElmer Inc., USA) with a 30 °C/min heating rate up to 800 °C under Ar gas flow at 100 ml min^{-1}. To evaluate the phytochemicals' role in α-MoO_3 NPs synthesis, fourier transforms infrared (FTIR) spectra were recorded from 400 – 4000 cm^{-1} (Shimadzu FTIR, Kyoto, Japan). The synthesised α-MoO_3 NPs were characterised for phase structure and crystallite size using powder X-ray diffractometer (XRD, X'Pert3 Powder, PANalytical, Netherlands) which was operated at 40 kV voltage and 30 mA current, using monochromatic radiation (Cu-Kα, 1.5406 Å) with nickel monochromator, and diffraction angle in the 10 – 70° range. The Scherrer equation ($D = K\lambda/\beta \cos\theta$) was used to determine the crystallite size. The morphology, size, and chemical composition of the synthesised nanoparticles were examined using a field-emission scanning electron microscope (FE-SEM, QUANTA FEG250) attached with energy-dispersive X-ray (EDX, Inspect S50, FEI, Netherlands) which was operated at 20 kV accelerating voltage, 10 mm working distance and probe current of 1.0 nA. For particle size and shape analysis, HR-TEM was employed. The specific surface area was measured with a BEL SORP-MAX analyser (MicrotracBEL, Japan). The Cd (II) concentration was analysed by atomic absorption spectroscopy (Perkin Elmer Model 3110) using air acetylene flame. To confirm cadmium loading on α-MoO_3 NPs surface, X-ray fluorescence (XRF) was measured using (JEOL JSM-6480, Japan).

3. Results and discussion

3.1. Structural and morphological characterisation of α-MoO_3

The XRD pattern of the synthesised α-MoO_3 NPs is shown in figure 1(A) and the inset. It can be indexed to the orthorhombic phase of α-MoO_3 with well-defined diffraction peaks at 12.8°, 23.4°, 25.8°, 25.9°, 33.8°, 39.1°, 39.7°, 45.9°, 46.4°, 49.3°, 50.2°, 51.7°, 52.9°, 54.2°, 55.2°, 56.4°, 57.8°, 59°, 61.8°, 63°, 64.6°, 65.1°, 66.9° and 67.7° which correspond to (2 0 0), (1 0 1), (4 0 0), (2 0 1), (1 1 1), (6 0 0), (5 0 1) (0 0 2), (6 1 0), (0 2 0), (3 0 2), (7 0 1), (1 12), (2 1 2), (1 2 1), (4 2 0), (7 1 1), (8 1 0), (6 0 2), (5 1 2), (6 2 0), (9 0 1), (7 0 2) and (10 0 0) planes, respectively. This pattern is in good agreement with COD Card No. 1537654 with corresponding lattice parameters $a = 13.825$, $b = 3.694$ and $c = 3.954$, and spacing group (P n m a (62)). The calculated crystallite size using Scherrer's equation was found to be 51.7 nm.

The surface morphology of the as-synthesised α-MoO_3 NPs was studied by FE-SEM as shown in figure 1(C). This image clearly shows the aggregates of α-MoO_3 NPs with spherical shapes. EDX analysis was recorded in the binding energy region of 0 – 10 keV (figure 1(B)) and shows the presence of Mo and O elements with ratios comparable to the theoretically calculated values confirming the purity of synthesised MoO_3 NPs. The TEM image (figure 1(D)) shows the

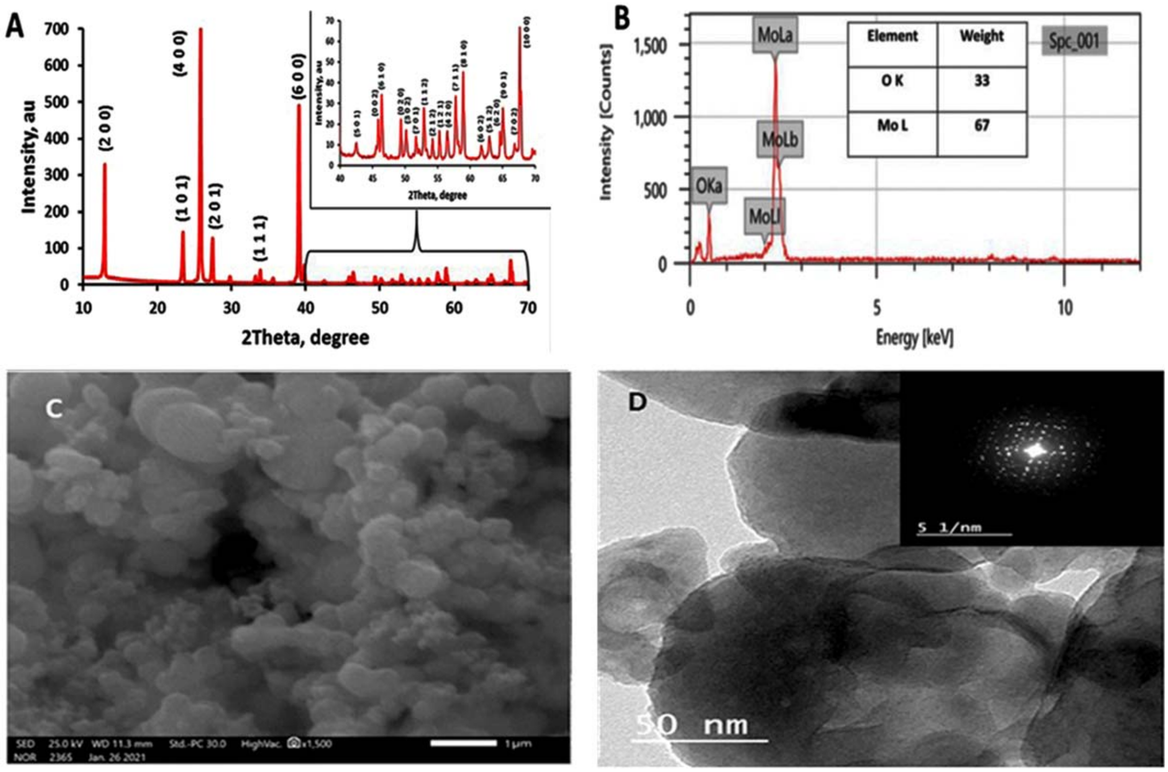

Figure 1. (A) XRD pattern, (B) EDX spectrum, (C) SEM image, (D) HRTEM image and SAED pattern of α-MoO_3 NPs (D inset).

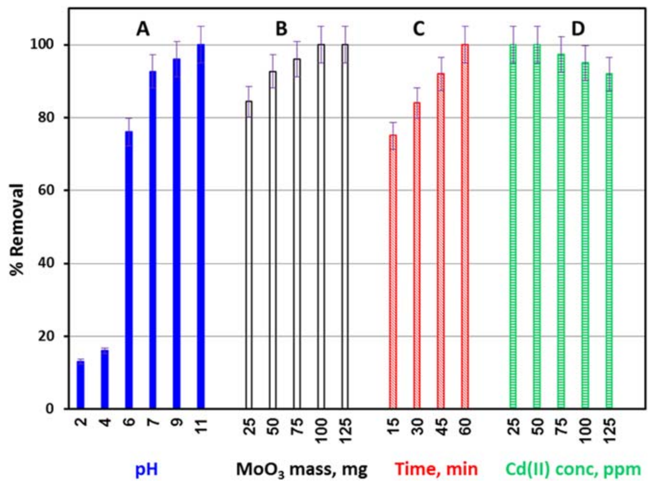

Figure 2. Effect of (A) initial pH, (B) α-MoO_3 NPs adsorbent dosage, (C) contact time, and (D) initial Cd (II) concentration on the adsorption process.

α-MoO_3 NPs aggregates with an average particle size of about 50 nm comparable with XRD results. The selected area electron diffraction (SAED) pattern (inset in figure 1(D)) reveals the crystalline nature of the α-MoO_3 NPs.

3.2. Adsorption studies

3.2.1. Effect of pH. The impact of pH values on the removal efficiency of 50 ml Cd (II) solution (50 mg l^{-1}) onto α-MoO_3 NPs (50 mg) is shown in figure 2(A). The increase in the solution pH from 2 to 11 resulted in an increase in the removal efficiency from 13 to 100%. The adsorbent surface is positive and consequently, adsorption of Cd (II) decreases at pH < 5.8 (PZC of α-MoO_3). By contrast, at pH > 5.8 α-MoO_3 surface is negative and thus Cd (II) adsorption increases [13]. Also, at high pH, the dissociation of surface hydroxyl groups of α-MoO_3 increases leading to the subsequent formation of low solubility Cd (II) species such as $Cd(OH)^+$ and $Cd(OH)_2$, and thus, Cd (II) removal increases. Solution pH should not be lower than 4 because of the possible dissolution of α-MoO_3 NPs. At pH > 8, various Cd hydroxide species [i.e. $Cd(OH)^+$, $Cd_2(OH)^{3+}$, $Cd(OH)_2$, $Cd(OH)_5^{3-}$ and $Cd(OH)_4^{2-}$] may be formed and transported into α-MoO_3 pores and thus might have contributed in Cd (II) removal [31]. Therefore, pH 7 (93% removal) was selected as the optimum pH value for the adsorption of Cd (II) onto α-MoO_3 NPs.

3.2.2. Effect of MoO_3 dosage. Adsorbent dosage is a vital parameter that determines the optimum adsorbent loading required for the complete removal of pollutants from the solution [13]. The influence of α-MoO_3 NPs dose (0.5–2.5 g l^{-1}) on cadmium removal was studied using 50 ml of Cd (II) solution (50 mg l^{-1}), pH 7, and agitation time 1 h at room temperature (25 °C). Results are depicted in figure 2(B) which shows a proportional increase in the removal efficiency with an increase in the α-MoO_3 NPs dose. It increases from 84.4% to 100% by increasing α-MoO_3 NPs dose from 0.025 g to 0.1 g. Increasing the adsorbent dosage increases the surface area and the available active sites, and consequently increases Cd (II) adsorption [31, 32]. Moreover, a further increase in α-MoO_3 NPs dosage beyond 0.1 g (at fixed initial cadmium concentration) does not affect adsorption wherever the removal efficiency already reached 100%. Thus, an adsorbent dosage of 0.1 g α-MoO_3 in 50 ml of Cd (II) solution (50 mg l^{-1}) was selected as the optimum adsorbent dosage for further experiments.

3.2.3. Effect of contact time. The equilibration time for maximum adsorption of Cd (II) onto α-MoO_3 NPs and the kinetics of the adsorption process were evaluated under optimised conditions: 50 ml of 50 mg l^{-1} Cd (II) solution, pH 7, 0.1 g α-MoO_3 NPs at 25 °C. Results are shown in figure 2(C). It exhibits quite rapid adsorption of Cd (II) by α-MoO_3 NPs in the beginning (75% within 15 min), followed by a slower removal (from 75% to 100% within 45 min) that gradually reached a plateau. The maximum removal of Cd (II) was achieved within 1 hr, and then equilibrium was attained. Thus, 1 hr was selected as the equilibration period for further experiments. The initial increase in the cadmium uptake may be due to a large number of available active surface sites on α-MoO_3 NPs for adsorption, and the high Cd (II) concentration gradient between solution and α-MoO_3 NPs surface. In the later stage, the Cd (II) adsorption is gone slowly due to saturation of vacant adsorption sites and the repulsion between Cd (II) ions on α-MoO_3 NPs surface and in the solution. The obtained results indicate that the α-MoO_3 NPs possess superior adsorption performance.

3.2.4. Effect of initial Cd(II) ion concentration. To evaluate the influence of initial Cd (II) concentration in the adsorption process, the experiments were conducted with different initial Cd (II) concentrations at a constant adsorbent dose (2.0 g l^{-1}), pH (7), contact time (60 min), and temperature (25 °C). Cadmium is completely removed at 25 and 50 mg l^{-1} initial concentration. Further increase in the concentration by 1.5 times resulted in the slight decrease of removal efficiency by 8% reaching 92% at 125 mg l^{-1} (figure 2(D)). This decrease in cadmium uptake by α-MoO_3 NPs may be associated with the saturation of the most active sites on the adsorbent surface at higher concentrations and the increase in the diffusion rate of Cd (II) into these sites to saturate them [33]. When the concentration is high, the adsorbent gets exhausted very fast thereby reducing the cadmium removal efficiency of the adsorbent. Conclusively, the adsorption of Cd (II) onto α-MoO_3 NPs and its mechanism are affected by initial cadmium concentration.

3.2.5. Adsorption isotherms. Langmuir and Freundlich's isotherms have been widely used for modelling adsorption data to understand the adsorbate/adsorbent interaction [31, 33]. Thus, they are used to fit experimental data obtained at Cd (II) concentrations from 25 mg l^{-1} to 125 mg l^{-1}. The linearised form of Langmuir equation is as follows

$$C_e/q_e = (1/K_L \cdot q_m) + (C_e/q_m), \tag{1}$$

where C_e (mg l^{-1}) and q_e (mg g^{-1}) are the equilibrium concentrations in liquid and solid phases, respectively, q_m (mg g^{-1}) is a Langmuir constant that expresses the maximum Cd (II) monolayer coverage capacity, K_L (l mg^{-1}) is Langmuir constant related to the energy of adsorption and affinity of the sorbent. The constants q_m and K_L are calculated from the slope and intercept of the linear plot of C_e/q_e versus C_e. The dimensionless separation factor or equilibrium parameter (R_L) of the Langmuir isotherm model can be calculated from equation (2) [34, 35].

$$R_L = 1/(1 + K_L C_0), \tag{2}$$

where C_0 is the initial cadmium concentration. The parameter R_L indicates the shape of isotherm and can take the values $0 < R_L > 1$; $R_L > 1$; $R_L = 1$ or $R_L = 0$ denoting favourable, unfavourable, linear or non-linear adsorption processes, respectively [32].

The linear form of the Freundlich equation can be written as equation (3):

$$\log q_e = 1/n(\log C_e) + \log K_f, \tag{3}$$

where K_f and n are the Freundlich constants which represent adsorption capacity and adsorption intensity, respectively. The value of n is calculated from the slope of the Freundlich linear plot (log q_e versus log C_e), while K_f is calculated from the intercept value. The linearised plot of Langmuir and Freundlich equations for cadmium ions adsorption on α-MoO_3 NPs at fixed temperature are presented in figures 3(A) and (B), and their constants with correlation coefficients (R^2) are tabulated in table 1. Langmuir and Freundlich plots have good linearity. The two models described the sorption isotherm well with the Langmuir model providing a slightly higher correlation ($R^2 = 0.98$) than the Freundlich model ($R^2 = 0.90$). Therefore, cadmium is probably chemically adsorbed in the form of a monolayer on α-MoO_3 NPs surface [13]. The maximum Langmuir adsorption capacity (q_m) by α-MoO_3 NPs was 57.5 mg g^{-1} at 25 °C. The calculated value of Langmuir affinity constant K_L is 2.3 l mg^{-1} indicating the good affinity of Cd (II) ions towards α-MoO_3 NPs. Langmuir adsorption intensity R_L values of 0.017 to 0.003 at different initial Cd (II) concentrations from 25 mg l^{-1} to 125 mg l^{-1} are plotted in figure 3(C). These values are between 0 and 1, indicating favourable and spontaneous adsorption of Cd (II) onto α-MoO_3 NPs which may partially occur by electrostatic interaction. Besides, Freundlich isotherm constant n is 9.3 ($n > 1$), indicating an effective Cd (II) adsorption process. Moreover, the high K_f value (39.8 mg g^{-1}) reveals the high adsorption capacity of α-MoO_3 NPs. In summary, all the above results confirm the favourability and effectiveness of Cd (II) adsorption onto α-MoO_3 NPs and it can occur via chemical bonding and electrostatic attraction.

3.2.6. Kinetic studies. The pseudo-first-order, pseudo-second order, and intraparticle diffusion models [34] are used to test the experimental data. These models provide some insight into the adsorption mechanism and the affinity of the adsorbent. The linear form of Lagergren first order is

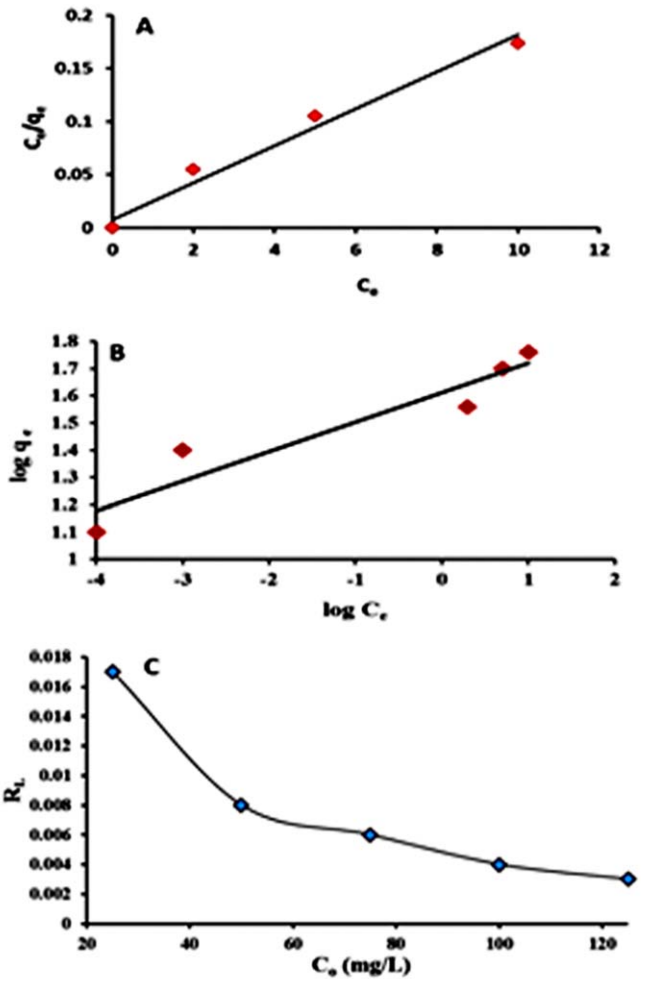

Figure 3. (A) Langmuir plot of C_e versus C_e/q_e, (B) Freundlich plot of log C_e versus log q_e, and (C) variation of adsorption intensity (R_L) with Cd (II) initial concentration for cadmium adsorption onto α-MoO_3 NPs at 25 °C (adsorbent dose (2.0 g l^{-1}), pH (7), and contact time (60 min)).

equation (4):

$$\log(q_e - q_t) = \log q_e - (K_1/2.303)t, \quad (4)$$

where q_e and q_t (mg g^{-1}) are the amounts of adsorbate per amount of adsorbent at equilibrium and at any time t and K_1 (min^{-1}) is the rate constant and can be calculated from the slope of the linear plot of $\log(q_e - q_t)$ versus time t, while the intercept represents q_e as illustrated in figure 4(A). The linear form of pseudo-second order is equation (5):

$$t/q_t = 1/K_2 {q_e}^2 + 1/q_e, \quad (5)$$

where K_2 (g mg^{-1} min^{-1}) is the rate constant of the pseudo-second-order model. The constants K_2 and q_e of the pseudo-second-order model are calculated from the slope and intercept of the linear plot of t/q_t versus time as shown in figure 4(B).

Weber and Morris equation for intraparticle diffusion model is described by equation (6) and shown in figure 4(C).

$$q_t = k_{ad} t^{0.5} \quad (6)$$

where q_t is the amount of cadmium adsorbed on the surface of α-MoO_3 NPs (mg g^{-1}) and K_{ad} is the intraparticle diffusion rate constant (mg g^{-1} $min^{0.5}$). Table 1 summarises the calculated constants and R^2 values of the three models. Pseudo-second order model ($R^2 = 0.992$, $q_e = 27.7$ mg g^{-1}) fits Cd (II) adsorption better than pseudo-first-order model ($R^2 = 0.990$, $q_e = 12.6$ mg g^{-1}) due to its higher R^2 value and its closer q_e value to the experimental q_e (exp.) (25 mg g^{-1}). This result indicates that Cd (II) adsorption onto α-MoO_3 NPs is probably controlled by chemical adsorption.

Intraparticle diffusion model plot in figure 4(C) showed two distinct linear portions and the intercept of the plot does not pass through the origin. This indicates the existence of more than one kinetic stage and that the intraparticle diffusion is not the only rate-limiting step in Cd (II) adsorption process. The presence of two straight lines in figure 4(C) indicates that the overall rate of Cd (II) adsorption process can be described by two distinct steps; mass transfer and intraparticle diffusion processes [36].

3.2.7. Adsorption thermodynamics. To understand the effect of temperature on the adsorption of Cd (II), experiments were conducted at the temperature values (25, 35, 45, and 55 °C) and the resulting Cd (II) removal efficiencies were 84.4, 86.5, 89, and 92%, respectively (figure 5(A)). The increase in adsorption efficiency by increasing temperature might be due to increased interaction between Cd (II) ions and active site on α-MoO_3 NPs surface, indicating that the adsorption process is endothermic [5, 13]. Gibb's free energy ΔG^0 in kJ mol^{-1}, the enthalpy ΔH^0 in kJ mol^{-1}, and the entropy ΔS^0 in kJ mol^{-1} K^{-1} were calculated at the above-mentioned temperature values using initial Cd (II) concentration of 50 mg l^{-1} and α-MoO_3 NPs mass of 0.025 g according to equations (7) – (9) [5, 37].

$$\ln K_c = (\Delta H^0/RT) + C, \quad (7)$$

$$\ln K_c = (-\Delta H^0/RT) + (\Delta S^0/R), \quad (8)$$

$$\Delta G^0 = -RT \ln K_c, \quad (9)$$

where, R is the universal constant (8.314 J mol^{-1} K^{-1}) and T is the absolute temperature (K). Equation (10) is used to calculate the thermodynamic equilibrium constant (K_c) in L g^{-1} for cadmium adsorption onto α-MoO_3 NPs.

$$K_c = C_s/C_e, \quad (10)$$

where, C_s is the equilibrium Cd (II) concentration adsorbed onto α-MoO_3 (mg g^{-1}) and C_e is the equilibrium concentration in solution (mg l^{-1}). Van't Hoff linearised plot of ln K_c versus $1/T$ (equation (8)) is shown in figure 5(B) and values of the thermodynamic parameters are given in table S1 (available online at stacks.iop.org/ANSN/12/035007/mmedia). The values of ΔH^0 (20.429 kJ mol^{-1}) and ΔS^0 (0.113 kJ mol^{-1} K^{-1}) were positive and ΔG^0 (-13.161, -14.29, -15.419, and -16.548 kJ mol^{-1} at 298, 308, 318, and 328 K, respectively) were negative. The positive value of ΔH^0 indicates an endothermic nature of the adsorption process [37]. Further, the positive ΔS^0 value reveals the increased randomness at the solid/solution interface [5, 37]. The ΔG^0 values decreased with an increase in temperature. The

Table 1. Langmuir, Freundlich, pseudo-first-order, pseudo-second order, and intraparticle diffusion model constants for cadmium adsorption onto α- MoO_3 NPs at 25°C.

Freundlich constants				Langmuir constants				
n	$1/n$	K_f	R^2	q_m	K_L	R^2		
9.3	0.1072	39.8	0.90	57.5	2.3	0.98		
Pseudo-first order			Pseudo-second order			Intraparticle diffusion		
K_1	q_e	R^2	K_2	q_e	R^2	K_{ad}	R^2	q_e (Exp)
0.041	12.6	0.990	0.004	27.7	0.992	6	0.93	25

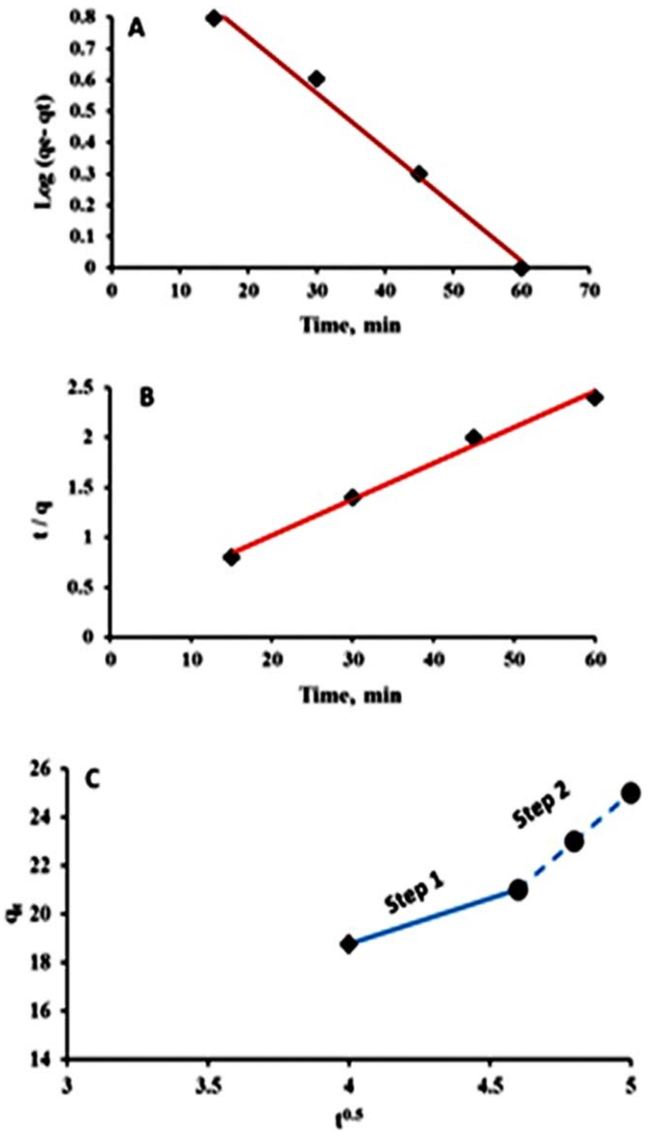

Figure 4. Linear plots of (A) Lagergren pseudo-first-order, (B) pseudo-second order, and (C) Weber and Morris intraparticle diffusion equations for cadmium adsorption onto α-MoO_3 NPs at 25 °C (adsorbent dose (2.0 g l^{-1}), pH (7), and contact time (60 min)).

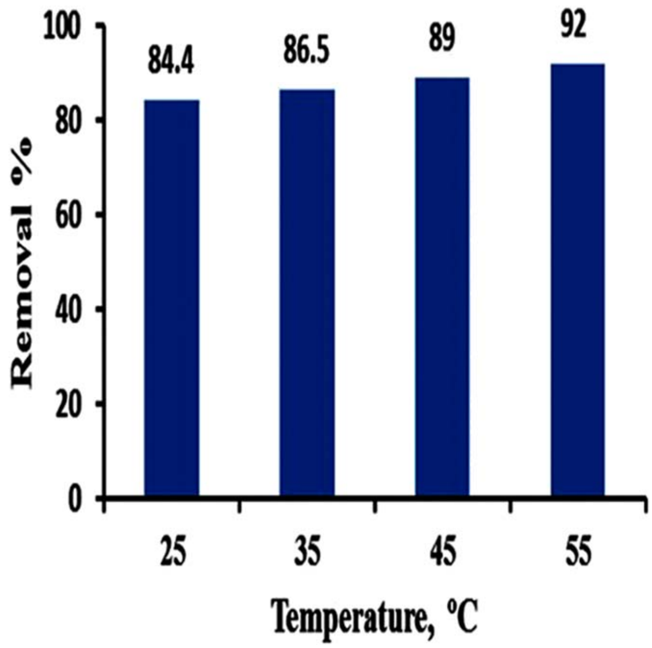

Figure 5. (A) Effect of temperature and (B) Van't Hoff plot of Cd (II) adsorption onto α-MoO_3 NPs (adsorbent dose (0.5 g l^{-1}), pH (7), contact time (60 min), and initial concentration (50 mg l^{-1})).

negative values of ΔG^0 indicate that adsorption was spontaneous and thermodynamically favourable.

3.2.8. Regeneration and stability. An ideal adsorbent should have not only excellent adsorbent storage ability but also very good desorption performance, which will greatly reduce the total cost of the water treatment process. EDTA and dilute inorganic acids such as HCl and HNO_3 have been used to desorb adsorbed heavy metals and regenerate the adsorbent [5, 34, 38]. EDTA can form steady complexes with metal ions while inorganic acids act mainly by the ion exchange mechanism. Regeneration using inorganic acids can lead to mass loss and some damage in adsorbent structure [38]. Thus, a 0.01 M EDTA solution was chosen for the regeneration of α-MoO_3 NPs. The results of five adsorption/desorption cycles are shown in figure 6(A). The removal efficiency decreased by only 3%; from 100% in the first cycle to 97% in the fifth cycle, indicating that α-MoO_3 is highly stable. The adsorbent stability was further examined by XRD analysis of α-MoO_3 NPs before and after Cd (II) adsorption as depicted in figure 6(B). It can be noted that α-MoO_3 is stable with no change in its crystal structure after regeneration.

3.2.9. Comparison with other adsorbents. The q_m values and experimental conditions of previously reported MONPs are

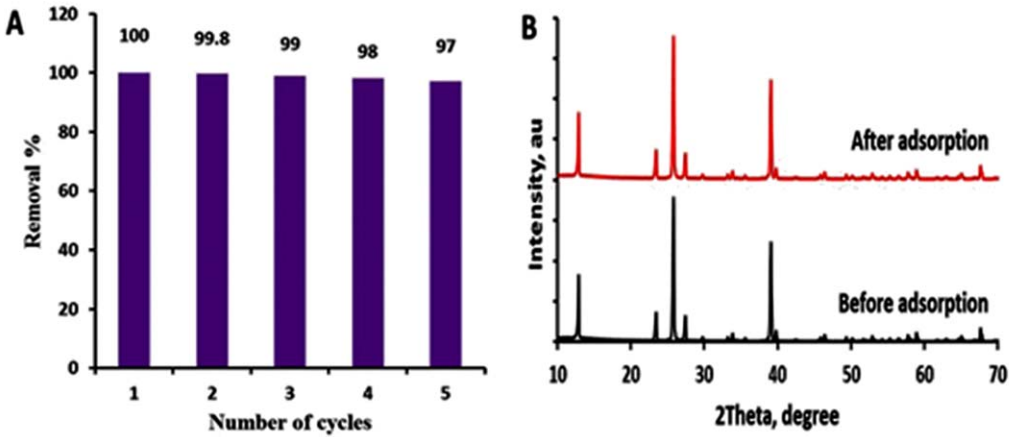

Figure 6. (A) Removal efficiency of Cd (II) onto α-MoO_3 NPs after five cycles (adsorbent dose (2.0 g l^{-1}), pH (7), contact time (60 min), and initial concentration (50 mg l^{-1}) at 25 °C), and (B) XRD patterns of α- MoO_3 NPs before and after Cd (II) adsorption.

listed in table S1. The as-synthesised α-MoO_3 showed the highest q_m value (57.5 mg g^{-1}) in the least contact time (60 min) compared with all green synthesised MONPs (15.5 – 37 mg g^{-1} in 120 – 240 min). It is also better than some chemically synthesised MONPs (1.2 – 44.4 mg g^{-1}). However, green synthesis has many advantages over chemical methods such as low cost, simplicity, and environmental friendliness. Another advantage of this adsorbent is its selective Cd (II) adsorption. Thus, α-MoO_3 is an excellent adsorbent for selective adsorption of Cd (II) ions from various aqueous media.

4. Conclusion

In this work, mesoporous α-MoO_3 NPs were green synthesised using buckthorn leaves and applied for Cd (II) removal from aqueous solutions by adsorption. 50 mg l^{-1} of Cd was removed within 1 hr using 0.1 g of α-MoO_3 at pH 7 and 298 K. At these optimised conditions, the maximum adsorption capacity was 57.5 mg g^{-1}. The experimental data were well fitted by pseudo-second-order and Langmuir models. Besides, the adsorption process was thermodynamically spontaneous (negative ΔG^0) and endothermic (positive ΔH^0). The selective adsorption of Cd (II) onto α-MoO_3 adsorbent was confirmed from the adsorption capacity results of coexisting ions. As a proof of α-MoO_3 stability, regeneration tests illustrated that the removal efficiency was slightly decreased by 3% after 5 adsorption/desorption cycles. Also, results indicated that the adsorption mechanism was likely chemical through complexation and electrostatic attraction. Thus, the biosynthesised α-MoO_3 is an eco-friendly nanoadsorbent for the selective removal of Cd (II) from aqueous solutions.

References

[1] Tahoon M A, Siddeeg S M, Salem Alsaiari N, Mnif W and Ben Rebah F 2020 *Processes* **8** 645
[2] Borji H, Ayoub G M, Bilbeisi R, Nassar N and Malaeb L 2020 *Water Air Soil Pollut.* **231** 330
[3] Motlochová M, Slovák V, Plížingrová E, Lidin S and Šubrt J 2020 *RSC Adv.* **10** 3694
[4] Visa A, Maranescu B, Lupa L, Crisan L and Borota A 2020 *Nanomaterials* **10** 899
[5] Zhang W, An Y, Li S, Liu Z, Chen Z, Ren Y and Wang X 2020 *Sci. Rep.* **10** 19549
[6] Zhang S, Cui M, Chen J, Ding Z, Wang X, Mu Y and Meng C 2019 *Mater. Lett.* **236** 233
[7] Sumisha A, Arthanareeswaran G, Thuyavan Y L, Ismail A F and Chakraborty S 2015 *Ecotoxicol. Environ. Saf.* **121** 174
[8] Irshad M A, Shakoor M B, Ali S, Nawaz R and Rizwan M 2019 *Water Air Soil Pollut.* **230** 278
[9] Tavker N, Yadav V K, Yadav K K, Cabral-Pinto M, Alam J, Shukla A K, Ali F A and Alhoshan M 2021 *Polymers* **13** 234
[10] Jawed A, Saxena V and Pandey L M 2020 *J. Water Process. Eng.* **33** 101009
[11] Wadhawan S, Jain A, Nayyar J and Mehta S K 2020 *J. Water Process. Eng.* **33** 101038
[12] Singh S, Kapoor D, Khasnabis S, Singh J and Ramamurthy P C 2021 *Environ. Chem. Lett.* **19** 2351
[13] Alqadami A A, Naushad M, Ahamad T, Algamdi M, Alshahrani A, Uslu H and Shukla S K 2020 *Desalin. Water Treat.* **181** 355
[14] Hong J, Xie J, Mirshahghassemi S and Lead J 2020 *RSC Adv.* **10** 3266
[15] Huang H, Wang Y, Zhang Y, Niu Z and Li X 2020 *Open Chem.* **18** 97
[16] Xue Z, Liu N, Hu H, Huang J, Kalkhajeh Y K, Wu X, Xu N, Fu X and Zhan L 2019 *R. Soc. Open Sci.* **6** 182195
[17] Zhu Y *et al* 2020 *Molecules* **25** 18
[18] Sharma P K, Raghubanshi A S and Shah K 2020 *Environ. Nanotechnol. Monit. Manag.* **14** 100315
[19] Sharma P K, Raghubanshi A S and Shah K 2021 *Environ. Sci. Pollut. Res.* **28** 13439
[20] Felix A A, Silva R A and Orlandi M O 2020 *CrystEngComm.* **22** 4640
[21] Noby S Z, Wong K K, Ramadoss A, Siroky S, Hagner M, Boldt K and Schmidt-Mende L 2020 *RSC Adv.* **10** 24119
[22] Al-Alotaibi A L, Altamimi N, Howsawi E, Elsayed K A, Massoudi I and Ramadan A E 2021 *J Inorg Organomet Polym Mater.* **31** 2017
[23] Jain V M, Shah D V, Patel K K and Doshi Y 2021 *IOP Conf. Series: Materials Science and Engineering* 1126 *(Bristol)* (IOP Publishing) 012052

[24] Zamora-Romero N, Camacho-Lopez M A, Vilchis-Nestor A R, Castrejon-Sanchez V H, Aguilar G, Camacho-Lopez S and Camacho-Lopez M 2020 *Mater. Chem. Phys.* **240** 122163
[25] Karthiga R, Kavitha B, Rajarajan M and Suganthi A 2018 *J. Alloys Compd.* **753** 300
[26] Abinaya M, Saravanakumar K, Jeyabharathi E and Muthuraj V 2019 *J. Inorg. Organomet. Polym. Mater.* **29** 101
[27] Shaheen I and Ahmad K S 2020 *J. Sep. Sci.* **43** 598
[28] Shaheen I and Ahmad K S 2021 *J. Solgel. Sci. Technol.* **97** 178
[29] Naghmouchi S and Alsubeie M 2020 *Not Bot Horti Agrobot Cluj Napoca* **48** 1600
[30] Kadioglu O, Jacob S, Bohnert S, Naß J, Saeed M E, Khalid H, Merfort I, Thines E, Pommerening T and Efferth T 2016 *Phytomedicine* **23** 293
[31] Siddiqui M F, Khan E A and Alam Khan T 2019 *Environ. Prog. Sustain. Energy* **38** e13249
[32] Peng L, Zeng Q, Tie B, Lei M, Yang J, Luo S and Song Z 2015 *J. Colloid Interface Sci.* **456** 108
[33] Elkhatib E, Mahdy A, Sherif F and Elshemy W 2016 *J. Nanomater.* **2016** 8496798
[34] Egbosiuba T C, Abdulkareem A S, Kovo A S, Afolabi E A, Tijani J O, Bankole M T and Roos W D 2021 *Sci. Rep.* **11** 75
[35] Wu S, Xie F, Chen S and Fu B 2020 *Environ. Technol.* **41** 3219
[36] Egirani D E, Poyi N R and Shehata N 2020 *Int. J. Environ. Sci. Technol.* **17** 2443
[37] Tu Y J, You C F and Chang C K 2012 *J. Hazard. Mater.* **235** 116
[38] Wan S, Yu C, Li Y, Lu Z, Wang Y, Wang Y and He F 2021 *Chem. Eng. J.* **405** 126576